RSC Advances

This is an *Accepted Manuscript*, which has been through the Royal Society of Chemistry peer review process and has been accepted for publication.

Accepted Manuscripts are published online shortly after acceptance, before technical editing, formatting and proof reading. Using this free service, authors can make their results available to the community, in citable form, before we publish the edited article. This *Accepted Manuscript* will be replaced by the edited, formatted and paginated article as soon as this is available.

You can find more information about *Accepted Manuscripts* in the Information for Authors.

Please note that technical editing may introduce minor changes to the text and/or graphics, which may alter content. The journal's standard Terms & Conditions and the Ethical guidelines still apply. In no event shall the Royal Society of Chemistry be held responsible for any errors or omissions in this *Accepted Manuscript* or any consequences arising from the use of any information it contains.

ROYAL SOCIETY OF CHEMISTRY

www.rsc.org/advances

Crystalline Photoactive Copper Indium Diselenide Thin Films by Pulsed Laser Crystallization of Nanoparticle-Inks at Ambient Conditions

*Qiong Nian[1,2], Martin Y. Zhang[1,2], Dong Lin[1,2], Suprem Das[1], Yung C. Shin[3], Gary J. Cheng[1,2,3]**

[1] Birck Nanotechnology Center, Purdue University, West Lafayette, IN 47906

[2] School of Industrial Engineering, Purdue University, West Lafayette, IN 47906

[3] School of Mechanical Engineering, Purdue University, West Lafayette, IN 47906

* Corresponding author. Email: gjcheng@purdue.edu

Abstract

Direct pulsed laser crystallization (DPLC) of large area printed nanoparticle-inks is investigated to form crystalline copper indium diselenide (CIS) thin film. This technique has a great potential to be utilized in scalable device production due to its atmospheric processing and high yield rate. It is found CIS nanoparticles of 20nm-diameter can grow to micro scale large crystals in film after DPLC. The internal imperfections including grain boundary, inter crystal gaps and voids were reduced significantly. The effects of laser intensity and pulse number on the deposited thin film are investigated. The localized field enhancement around nanoparticle contacts is believed to be responsible for nanoparticles welding and crystal growth near CIS film surface area during DPLC. The complete crystallization of CIS nanoparticles along depth direction is attributed to thermal diffusion driven rapid melting/solidification. Moreover, it was found that the microstructure change in CIS film after DPLC influences the optical and electrical performance significantly. A typical increase of 7.9% (visible range) and 19.2% (near infrared range) in optical absorbance is obtained under optimal DPLC conditions and a Band-gap shrinkage (ΔE_g) of CIS thin film after DPLC leads to broader acceptance of solar spectrum of

RSC Advances Accepted Manuscript

100 nm. The results from Raman spectrum and Photoluminescence (PL) of thin films under various laser conditions reveal that the improvement of the optoelectronic properties of the CIS thin film is related to the reduction of crystal defect level in the thin film.

Key words: *direct pulsed laser crystallization, copper indium diselenide, photoactive nanoparticles, optical absorption, Raman spectrum, Photoluminescence.*

Introduction

Thin film solar cell has drawn much attention due to low material consumption and reliable device manufacturing techniques for large scale productions[1]. Its high efficiency (~19.9% based on copper indium gallium diselenide (CIGS) by National Renewable Energy Laboratory (NREL)[1]) and long-term stability are also of great interest in solar cell[2]. However, high production cost of current CIS film manufacturing still becomes one of the major obstacles for its wide range implementation[3]. A lot of efforts have been made to reduce the film fabrication cost, such as aqueous solution synthesis and doctor blade coating[3-5]. However, most present-day low cost fabricated photovoltaic device is inefficient, owing to the defects in copper indium diselenide (CIS) thin film crystalline structure. Grain boundaries, inter-crystal gaps and inter-nanoparticle voids increase nanometer and micrometer scale interfaces between crystalline domains, which play crucial roles in photovoltaic performance[6, 7].

In order to reduce the internal imperfections, various post crystallization techniques after low cost fabrication are developed to densify the film structure and increase grain size. Among them, rapid thermal annealing (RTA)[3] has been widely investigated, as well as Direct pulsed laser crystallization (DPLC)[8, 99] , for efficient and effective crystallization. However, RTA is

RSC Advances Accepted Manuscript

expensive to be scaled up in industry due to some intrinsic issues such as temperature required, quasi-static temperature change leading to poor control of grain size and use of costly vacuum/inert gas systems. In addition, RTA is a non-selective heating process, not suitable for cutting-edge low melting point and large area substrates. DPLC has several advantages such as: (1) *Processing speed and large area processing*: DPLC process make use of direct nanosecond-pulse laser interaction with target nanocrystals. If equipped with beam scanner (>10m/s) and commercial available diode pump solid state (DPSS) laser with frequency of 50-100 kHz, DPLC provides a fast speed, low cost, large area processing technique; (2) S*elective processing*: different materials absorb laser energy at different wavelengths, such as CIS at visible region, while transparent conductive layer (i.e. aluminum-doped ZnO) absorbs laser at ultraviolet region. By selecting appropriate laser wavelength, DPLC only selectively processes the target and keeps other materials intact, which might be able to boost cutting edge organic based devices[10-12] and solution based coatings[13-15]. Exploring ultra-fast laser beam with small heat effective zone for selective crystallization, this process is efficient, in micro second scale, as demonstrated in our prior works[16, 17].

In this study, the mechanism of laser nanoparticle interaction is systemically investigated in order to find out the effects of laser processing conditions on the crystallinity of the thin film. During DPLC, the contacts between nanoparticles are localized heated and jointed to form a large crystal. With number of pulse increases, the crystal size gets bigger and bigger due to reduction of surface energy in nanoparticles, grain boundaries, inter-crystal gaps and inter-nanoparticle voids, as schematically illustrated in Figure 1(a). Field emission scanning electron microscopy (FESEM) characterization in Figure 1(b) shows clear comparison before/after DPLC

RSC Advances Accepted Manuscript

under optimal processing conditions. The microstructures after DPLC will be analyzed to show their effects on optical and electrical properties of thin film.

Experimental methods

Before DPLC, chalcopyrite CIS nanoparticles and ink, which are suitable for scalable coating process, were synthesized via a facile solution method referring to prior advancements[3]. Briefly, first of all, a three-neck round bottom flask was degassed at ~130 ^{o}C for 30 minutes followed by purging with Ar gas several times. Then, 2.5 ml of 0.2 molar solution of CuCl, and 2.5 ml of 0.2 molar solution of InCl3, and 4 ml of 0.25 M Se suspension (all in oleylamine) were added to the flask for reaction. Next, the reaction mixture was heated to the 265 ^{o}C slowly for 1 hour and then held for 1 hour to let the particles grow. After the reaction, the nanocrystals are then collected by centrifuge and re-dispersed in toluene to form an ink. DPLC of CIS nanoparticles film is designed to operate at ambient conditions: room temperature and atmospheric pressure. Continuum Surelite^{TM} series Nd: YAG pulsed laser operated at second harmonic generation (SHG, 532nm) is used. This wavelength is chosen since CIS has a good absorbance at this wavelength, while other layers such as *i*-ZnO and TCO layers are transparent. The energy of incident laser (E = 2.3 eV) is almost double of the band gap energy of CIS (E_g = 1.04eV), sufficiently exciting the electrons in the CIS film and enabling the corresponding local heat generation. Single laser pulse duration is 5 ns, multi pulse is applied to achieve through thickness crystalline thin film. Laser intensity could be tuned by laser pulse energies and beam sizes, adjusted by the power attenuator and beam expander respectively (optimal laser intensity is 4.8MW/cm^2 with 30pulses). During DPLC, the CIS target sample is placed on a PC-controlled motorized stage to enable x-y translation.

RSC Advances Accepted Manuscript

After crystallization process, FESEM is utilized to observe the morphological features of the CIS thin film after DPLC. Both top surface and cross sectional morphology are characterized. Focused ion beam contrast channeling (FIBCC) technique is used to confirm the growth of CIS crystals by determining the grain size. Lambda 950 visible-Near Infrared (NIR) spectrophotometer is used to measure the transmittance and absorbance spectra of CIS, and accordingly band gap is determined by plotting the absorbance squared versus energy, and followed by extrapolation to zero. Properly calibrated D8 Focus X-ray Diffraction (XRD) facility (Bruker) is utilized to determine the maintained structural property of CIS processed by DPLC. Raman spectra are characterized by Confocal Raman microscope equipped with a motorized sample stage. Spectra Pro-300i is used to measure photoluminescence of DPLC processed CIS thin film.

Results and Discussions

As schemed in figure 1a and characterized in 1b, the cross-sectional view observes a large area CIS film of 20 μm × 2 μm. It clearly shows CIS film structure and component units from top to bottom surface. The CIS nanoparticles are coated on 1 μm thick Molybdenum to form photoactive film by doctor blade coating[3-5], before which Molybdenum is sputtered onto SLG to form back electrode. The processed and unprocessed area during DPLC is marked, between them, an apparent boundary line differentiate the crystallized film and residual nanoparticles. Subject to unprocessed area in Figure 1b, the nanoparticles packed together with residue solvent induced in synthesis and coating. These particles and agglomerated ones stacked into thick layer, thus inevitable inter-particle holes and voids are formed. However, subject to processed area, nanoparticles welded together and large crystals grown are achieved and difficult to find

RSC Advances Accepted Manuscript

nanoparticles residue through the whole film depth. This crystallization and inter-particle defects removal could be further verified by FESEM surface morphology comparison between figure 1c and figure 1d. VeecoTM optical profilometry is also used to determine the changes on surface roughness of CIS thin film as shown in figure 1c and 1d inserts. The surface roughness of the as-received sample was 347 nm and 437 nm for R_a (the arithmetic average of absolute surface roughness values) and R_q (the root mean square of absolute values), respectively; after DPLC, the R_a and R_q became 180 nm and 251 nm, respectively. The details of CIS film surface roughness and crystallinity improvement would also be investigated in next figures. The comparison strongly states the crystallization effect of DPLC under optimal conditions, which also could be demonstrated by the Raman spectrum (figure 1e) and Photoluminescence (PL) spectrum (figure 1f). The apparent Rama signal and PL response subject to crystallized samples reveal improved film quality and enhanced photo-response performance.

During DPLC, two processing parameters played important roles: laser intensity and pulse number. To investigate the optimal processing condition for CIS nanoparticles (*diameter* = 20~40 nm), a series of experiments were carried out. Figure 2 shows the effect of laser intensity on CIS film microstructure with fixed pulse number. For pulse number subject to 30, different laser intensities irradiated at the CIS thin film led to completely different surface morphology. When laser intensity was relatively low (2MW/cm^2), very few crystals grow occurred, as shown in Figure 2a. This was attributed to inadequate thermal energy causing insufficient crystal growth or crystal melting. When laser pulse with a higher intensity (3.2~3.8MW/cm^2) was applied, obvious growth occurs to most of crystals but still leave several discrete nanoparticles, as shown in Figure 2b and 2c. When 4.8 MW/cm^2 was applied, crystal growth occurs to almost all crystals.

RSC Advances Accepted Manuscript

The contact between nanoparticles was modified, resulting in good homogeneity and surface smoothness in Figure 2d. Thus, it was considered that 4.8 MW/cm^2 as the optimal intensity for current series of samples. However, higher laser intensity like 5.4 and 6.7MW/cm^2 would damage the film quality because of excess thermal energy in DPLC, for instance, the film would end up with either poor porous structure (Figure 2e) or ablation at the surface (Figure 2f). Neither of these two cases is favorable for CIS film practical application. The laser intensity effect mainly attributes to the peak temperature increase, where higher intensity brings more energy delivery which increases the peak temperature. If the peak temperature is too high, the CIS film would be vaporized or even ablated, resulting in poor film quality.

The effect of pulse number was characterized as presented in Figure 3, under fixed laser intensity of 4.8 MW/cm^2. Cross-section images in Figure 3 show that crystal growth occurs not only on top surface, but also along thickness direction. As compared between Figure 3a and 3b, in the first several pulses, oxygenic ligand and dispersant brought in synthesis and coating were removed, leading to close-packed and densified film structure. This initial laser pulses delivery eliminates the nanoparticles agglomeration, decreases the inter-particle gaps and benefits following crystallization. With more laser pulses coming in (10-20 pulse), the crystallization starts penetrating deeper to around 500 nm thick. Crystallization also could be demonstrated by the nanoparticles merging and large crystal forming, which is shown in Figure 3c and surface morphology insert. Along with multi-pulse delivery continues, such as 20-25 pulses applied, the crystallization thickness extends to almost through the whole film in Figure 3d. The crystallization penetrates deeper due to heat transfer along thickness, since gaps between nanoparticles are reduced by the first several pulses therefore heat diffuses more easily and CIS

RSC Advances Accepted Manuscript

film with bigger grains in top layer possesses higher thermal and electrical conductivities than CIS film with small grains[18]. With more laser pulses coming in, the more grown crystals on top conduct thermal energy at a faster rate within the thin film thereby boost the crystallization process (both population and depth). Finally, after 30 pulses, the crystal growth propagated through the entire thin film to form large crystals as seen in Figure 3e and surface morphology insert. Comparing Figure 3a to 3e, it clearly shows a great reduction of inner imperfections, such as gaps, voids and grain boundaries. The growth of crystals and decrease of inter-crystal gaps are confirmed by FIBCC technique[19, 20]. In Figure 3a, the as-received CIS film has a loose structure with nanocrystals size in 20-40 nm. As the first few laser pulses coming in, top surface small grains with different orientations were observed at 100 nm scale. However, random holes are still obvious which indicates that crystallization is incomplete, though obvious grain growth. After 30 laser pulses, the whole region of interests (ROIs with approximately length x thickness = 4 x 2 μm) showed homogeneity, neither holes nor inter-crystal gaps was observed in Figure 3f. IN addition, there is coherent boundary with the Mo layer underneath. This indicates the CIS nanocrystals grew up by merging with neighbor nanocrystals, thus inter-crystal gaps and void defects were overcome and large CIS crystals were formed.

To understand the interaction between CIS nanoparticles and pulse laser during DPLC, Comsol simulation was performed as shown in Figure 4a with essential science indicators presented in table 1[16, 21, 22]. The Laser pulse was modelled with a Gaussian electromagnetic wave as incident on a stack of nanoparticles. Gaussian beam laser was delivered with an electrical field of 1 V/m. Each nanoparticle was modelled as having a circular cross-section in diameter of 20nm with essential physical parameters input. The simulation provided local electric field strength

RSC Advances Accepted Manuscript

distribution in the stacked nanoparticles shown in Figure 4a, quantified by color legends. Local electrical field varied area to area, and concentrated as high as 14 V/m near contacts between nanoparticles due to Surface Plasmon Polarization[23, 24]. It is well deserved to note that mainly nanoparticles contacts are able to enhance the local electrical field and form 'hot spots', while leaving particles themselves in low strength field. To further explore the heating process generated by the 'hot spots', the heat generation distribution from area to area was plotted in Figure 4b contours. The heat generation was determined from the illumination power density multiplies the nanostructures absorption coefficient[25], that is, the power loss density calculated by Comsol Multiphysics®. As illustrated in Figure 4b, the power loss density concentrates near particle contacts, and decrease as distance to contact increasing. The highest power loss density at nanoparticle contacts reaches ~ 9.25 W/m^3, while inside nanoparticles only generate as low as ~ 1.05 W/m^3. It implies that the localized heating of the contacted region between nanoparticle/nanoparticle, and nanoparticles/large crystals is one of the reason for welding nanoparticles together during DPLC, boost crystal growth to form large ones and moreover reduce internal imperfections in CIS film like voids and gaps[26, 27].

These observations verified the mechanism of DPLC, which is in agreement with prior statements[8, 9]. During laser heating, photon energy is directly transferred to the electrons within a few picoseconds (ps), and resulted in heat leading to the melting of laser penetration depth region. Some other processes are considered in the heating: (1) Laser intensity may be concentrated near nanoparticle contacts, because of Surface Plasmon Polarization; (2) Laser with photon energy greater than the band gap of CIS may generate electron-hole pairs which may absorb laser energy and be excited to a higher excited state; (3) The laser photon can cause inter-band and

RSC Advances Accepted Manuscript

intra-band transitions which lead to the formation of dense and hot electron-hole solid state plasma. The heat would then be transferred into the sample, however with some delay due to heat diffusion. The heat diffused from surface through micrometers depth usually within 100ns[8, 9, 28]. The cooling occurred after the finish of laser pulse and heat propagation. Usually the cooling rate is proportional to the temperature gradient with a value up to 10^9 K/s at the surface and 10^8 K/s at 1 μm deep[9]. Heat diffusion, controlled by material properties (such as thermal conductivity, thermal diffusivity, and specific heat) governs the localized temperature raising and cooling. Heat diffusion governing equation can be written as[29]:

$$\frac{\partial T}{\partial t} = \frac{\partial}{\partial x}\left(\frac{\kappa}{\rho C_p}\frac{\partial T}{\partial x}\right) + \frac{\alpha I(x,t)}{\rho C_p} \qquad (1)$$

Where: T is the temperature field, κ is the thermal conductivity, $D = \kappa/\rho C_p$ is the thermal diffusivity, α is the light absorption coefficient, I is the laser intensity as a function of x inside the material and at time t. Assuming a Gaussian beam laser, The heat diffusion and temperature inside CIS film was stated with finite element analysis (FEA) in our prior development[26]. Within the heat diffusion and temperature increase, normal and abnormal crystal growth in thin films were reported[30]. The thermodynamic driving force of the grain growth differentiates them. Normal grain growth is driven by the minimization of total free energy of the system via the combination of neighboring grain boundaries thus increasing the grain size. The increase of grain size is continuous and forms a mono-modal grain size distribution. The maximum grain size is limited by the thickness of the film. Abnormal grain growth, on the other hand, is driven by surface and strain energy difference among neighboring grains. The magnitude of the difference determines the rate of grain growth. During abnormal grain growth, a small fraction of grains grows at a significantly higher rate compared to the others[31]. Abnormal grain growth stops when

RSC Advances Accepted Manuscript

secondary grains impinge on one another, therefore, the final grain size may be several times greater than the film thickness[32]. It is believed that abnormal crystal growth dominates the crystal growth of DPLC processing, as shown in Figure 3e.

To investigate the effect of film microstructure modification on CIS optical property, the absorbance spectra of as-received and DPLC-processed CIS-based absorber layer were measured by Lambda 950 spectrophotometer in the wavelength range 400-1200 nm, as shown in Figure 5a. DPLC-processed samples show obvious increase in absorbance throughout the visible to near infrared region (500-1200 nm), while less than 500 nm, a decrease in the absorbance is observed. In the range of 500 to 800 nm, optical absorbance has an average increase of 7.85% after DPLC treatment. It is worthy to point out that at the wavelength of 535 nm, there is a 5.2% increase in absorbance after DPLC treatment, this agrees with earlier reports[18, 33-35]. In the NIR (800 to 1200 nm) region as shown in Figure 5b, the DPLC-processed sample is at least 19.2% (average) higher absorbance than the as-received sample (i.e. 11.6% at 800 nm, 18.4% at 1000 nm, and 29.3% at 1200 nm). This implies that potentially DPLC might improve the external quantum efficiency of the CIS-based solar cells as it absorbs more solar radiation. The absorbance enhancement attributes to film microstructure modification such as densified film, uniform and homogeneous surface and reduced internal imperfections. Since the stoichiometry of CIS has been well maintained and no indication of thermal decomposition was found after DPLC processing, according to typical XRD spectrum shown in Figure 5a insert. The major diffraction peaks observed at 26.65°, 44.22°, 52.39°, 64.36°(2-Theta) can be indexed to the (112), (204)/(220), (116)/(312), (008)/(400) of the tetragonal crystal structure[3, 4], respectively.

RSC Advances Accepted Manuscript

Band gap (E_g), a crucial factor determining material optical absorption, could be approximated by plotting the absorbance squared versus energy, and then extrapolating to zero[3]. The band gap of as-received and DPLC-processed is determined to be 1.07 eV, and 1.01 eV, respectively, shown in Figure 5c. Both two measured values are in good agreement with the reported value of bulk α-CIS (1.04 eV)[3]. However, a small band gap shrinkage (ΔE_g = 60 meV) is observed after DPLC treatment, which widens the acceptable range of solar spectrum by 6% (extends from 1159 to 1228 nm). The absorbance increase and the band gap shrinkage suggest that DPLC-processed CIS thin films accept more solar irradiation compared with as-received films. The change of band gap and optical absorbance was observed by prior experimental and theoretical work reported in literature[36]. It is found that band gap shrinkage strongly depends on the carrier concentration density (n). The relation between band gap shrinkage and carrier concentration is proposed by Burstein[37] and Moss[38] with B-M model which states that the band gap shrinkage (ΔE_g) changes with the carrier concentration in the conduction band, as stated in Eq. (2)[39].

$$\Delta E_g = \left(\frac{3}{8\pi}\right)^{2/3}\left(\frac{h^2}{2m_e}\right)n^{2/3} \qquad (2)$$

Where: h is Plank constant, and m_e represents effective mass of carrier (g). In order to quantify the band gap shift, the carrier concentration should be measured first. Refer to our prior report, carrier concentration decreases slightly from $1.681\text{x}10^{18}$ to $1.493\text{x}10^{18}$ (cm^{-3}) after DPLC process. Substituting values in Eq. (2) with measured carrier concentration density n=1.493 $\text{x}10^{18}$ cm^{-3}, band gap shrinkage (ΔE_g) is then calculated to be 57.6 meV. This agrees well with the ΔE_g = 60 meV drawn from optical measurements. This is ascribed to the diffusion of copper combined with the fact that the carrier effective mass of CIS is small, makes the conduction band carriers to degenerate at a relatively low concentration, causing a shift in Fermi level as well as

RSC Advances Accepted Manuscript

band gap[40]. Hall Effect measurements also demonstrate two orders enhancement on hall mobility and boost on photocurrent collection[16].

In order to understand the mechanism of DPLC, a systematic study was conducted to determine the optimal laser condition. The approach could be also applied to other nanoparticles to form crystallization thin films. The typical Raman spectra of CIS thin films processed by DPLC with different laser intensities and pulse numbers were collected and shown in Figure 6. As observed, A1 peak located at $175cm^{-1}$, which is normally observed in I-II-VI_2 chalcopyrite compounds[39, 41]. The weak peaks located at $129cm^{-1}$ and $213cm^{-1}$ are corresponding to the single phase chalcopyrite structure CIS[42]. The peak located at the highest wave number position $261cm^{-1}$ is originated from the secondary phase such as copper selenite[43]. According to[41, 44], the appearance and intensity of A1 peak is strongly dependent on crystallinity of CIS thin film including crystal size, orientation and crystalline ordering; on the other hand, the presence of the secondary phase peak indicates highly disordered crystalline. In Figure7(a), comparing with as-received sample, A1 peak of DPLC processed CIS films become stronger and secondary phase peak became weaker with higher laser intensity. This reflects a better film crystallinity and a trend to growth of the large mono-crystalline grains. However too high laser intensity like 6.7 MW/cm^2 will ablate CIS thin film to generate worse film crystal quality, whose A1 peak became weaker and secondary phase peak become stronger. Figure 6(b), (c) and (d) show pulse number effect of laser intensities of 3.8 MW/cm^2, 4.8 MW/cm^2 and 5.4 MW/cm^2, respectively. For two lower laser intensities 3.8 MW/cm^2 and 4.8 MW/cm^2, 50 and 30 pulses are required to get good film crystallinity. On the other hand, for laser intensity of 5.4 MW/cm^2, 5 pulses is enough to supply thermal energy for recrystallization, while more pulses will introduce negative effect. Comparing

RSC Advances Accepted Manuscript

the spectrum together in same scale, we can find 4.8 MW/cm^2, 30 pulses the optimal condition for DPLC processed CIS film. Comparing Raman spectra of CIS processed by 3.8 MW/cm^2 to as-received sample in Figure 6(a), a slight 2 cm^{-1} A1 peak shift away from 175cm^{-1} was observed, which is also an indication of growth material referring to Zaretskaya etc.[41].

The crystallinity changes are concomitant with an improvement of the optoelectronic properties of the CIS thin film. Thus, typical room temperature photoluminescence (PL) could also be used to determine optimal condition. Figure 7(a) presents the spectra of the 2 um thick CIS thin films processed by DPLC with different laser intensities and 30 pulses. As shown in this figure, the peak of the as-received CIS thin film locates around 1200 nm, meaning the band gap is approximately 1.04 eV[3, 45]. However, the peaks of the recrystallized CIS thin films shift small amount to longer wavelength (lower energy) with increasing laser intensity. This is an indication of small band gap shrinkage of DPLC processed CIS thin film. This shrinkage is originated from carrier concentration drop after DPLC[37, 38, 40], which agrees well with Absorbance spectra and Hall Effect analysis in table 2. On the other hand, according to[46], PL peak intensity strongly depends on surface carrier recombination process, relating with CIS thin film crystallinity and inter-grain defects level. With better film crystallinity and lower inter-grain defects density, it is easier for separated carriers diffusing to film surface for recombination, which will increase PL peak intensity.

Comparing with as-received sample, the DPLC processed CIS thin films show stronger PL peak with increasing laser intensity in Figure 8 (a). We find 4.8 MW/cm^2, 30 pulses is optimal

RSC Advances Accepted Manuscript

condition to obtain strongest PL peak implying most improved CIS film. With too high laser intensity, such as 5.4 MW/cm^2, a weak PL peak is observed. The decreasing PL peak intensity majorly attributes to import non-radiative recombination and rather poor film crystallinity[47]. This poor film crystallinity results from that the excess thermal energy will ablate thin film[48].

Figure 7(b), (c) and (d) present pulse number effect affected by laser intensity. For laser intensity of 4.8 MW/cm^2, 30 pulses is optimal for DPLC presented in Figure8 (c).Too many pulses will ablate thin film and then degrade film crystal quality, bringing weaker PL peak. However, for lower laser intensity like 3.8 MW/cm^2 shown in Figure 7(b), larger pulse number like 50 are needed to supply enough thermal energy for DPLC. Figure 7(d) shows 4.8 MW/cm^2, 30 pulses is the optimal condition for DPLC processed CIS film, which can mostly improve film crystallinity and lower inter-grain defects density to obtain strongest PL peak. This is in a good agreement with Raman spectra analysis.

Conclusions

In this study, a systematic study was conducted to understand the mechanism of DPLC of CIS nanoparticles-ink. During DPLC, 20nm-diameter CIS nanoparticles grow to micro scale large crystals in film. The internal imperfections including grain boundary, inter crystal gaps and voids were reduced significantly. It is found the microstructure and property of thin film largely depends on laser intensity and pulse number. The localized field enhancement around nanoparticle contacts is believed to be responsible for nanoparticles welding and crystal growth near CIS film surface area during DPLC. The complete crystallization of CIS nanoparticles along

RSC Advances Accepted Manuscript

depth direction is attributed to thermal diffusion driven rapid melting/solidification. Moreover, it was found that the CIS film microstructure change after DPLC influences the optical and electrical performance significantly by compensating the internal imperfections, such as: a typical increase of 7.9% (visible range) and 19.2% (near infrared range) in optical absorbance is obtained under optimal DPLC conditions and a Band-gap shrinkage (ΔE_g) of CIS thin film after DPLC leads to broader acceptance of solar spectrum of 100 nm. Systematic study is carried out by characterization and analysis of Raman crystallinity and PL of DPLC processed CIS thin films under various laser conditions, which confirms that the improvement of the optoelectronic properties of the CIS thin film is related to the reduction of crystal defect level in the thin film.

Acknowledgement

Financial support from NSF (CMMI 1030786) is appreciated. The authors would like to thank Dr. Qijie Guo for his generous support in preparing CIS nanoink thin films.

Table 1 Essential Physics Parameters Applied in COMSOL Multiphysics.

Laser parameters			**CIS properties**			
Wavelength (nm)	**Pulse width (ns)**	**Repetition Rate**	**Low frequency dielectric constant**	**High frequency dielectric constant**	**Density (g cm^{-3})**	**Carrier concentration density (cm^{-3})**
248	**25**	**10**	**8.1**	**13.6**	**5.77**	**1.68×10^{18}**

RSC Advances Accepted Manuscript

Figure 1

Figure 1: (a) Methodology of low cost DPLC of CIS thin film. (b) Cross sectional FESEM images shows different morphology of CIS thin film before (right) and after (left) DPLC processing. (c) Surface morphology of CIS thin film before DPLC. (d) Surface morphology of CIS thin film after DPLC. (e) Raman spectrum comparison between as-received CIS film and the crystallized one. (f) PL spectrum comparison between as-received CIS film and the crystallized one.

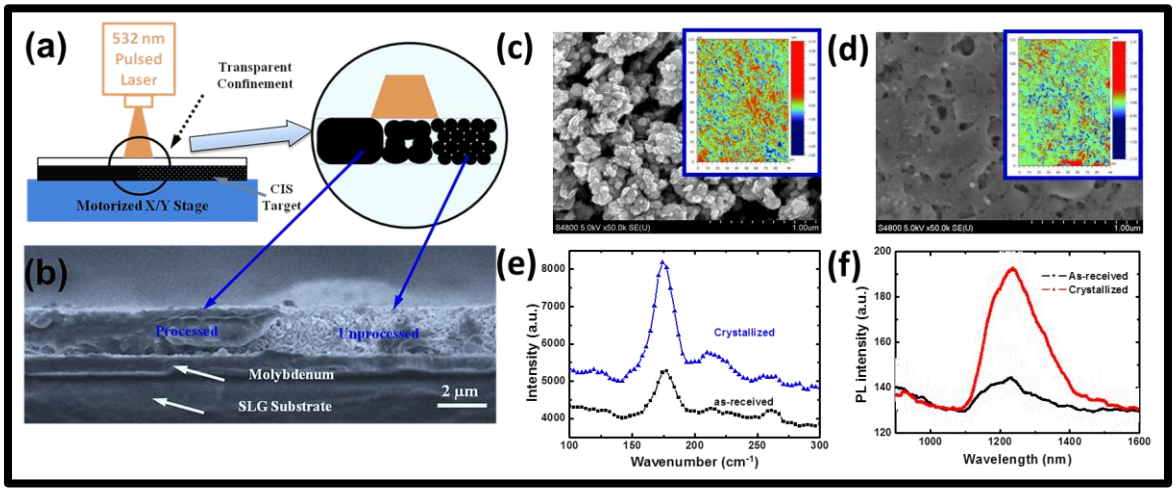

Figure 2

Figure 2: Top surface morphology when of CIS film treated with different laser intensities. Pulse number $N = 30$ for all six cases: (a) 2 MW/cm^2, (b) 3.2 MW/cm^2, (c) 3.8 MW/cm^2, (d) 4.8 MW/cm^2, (e) 5.4 MW/cm^2, and (f) 6.7 MW/cm^2.

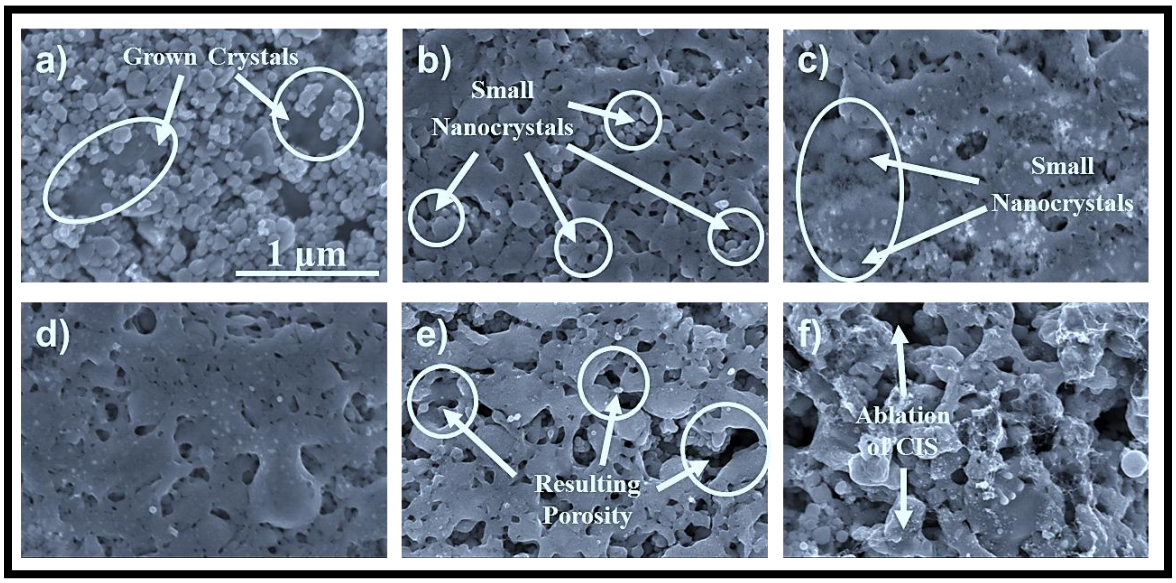

RSC Advances Accepted Manuscript

Figure 3

Figure 3: Effects of pulse number (*N*) on the crystallization of nanoparticles in depth direction. Images show cross section views of CIS film processed by DPLC with different pulse number, while inserts show FESEM observation on the top surface. Laser intensity was fixed at 4.8 MW/cm^2. (a): as-received, (b): 10 pulses, (c): 20 pulses, (d): 25 pulses, and (e): 30 pulses. (f) : Characterization of CIS grain size as a result of DPLC processing with 30 pulses by FIBCC technique taken from cross section of CIS thin films with 52^o degrees tilt:

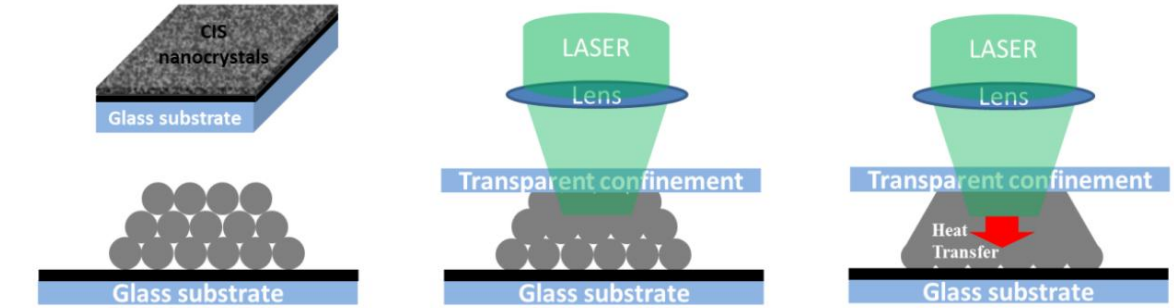

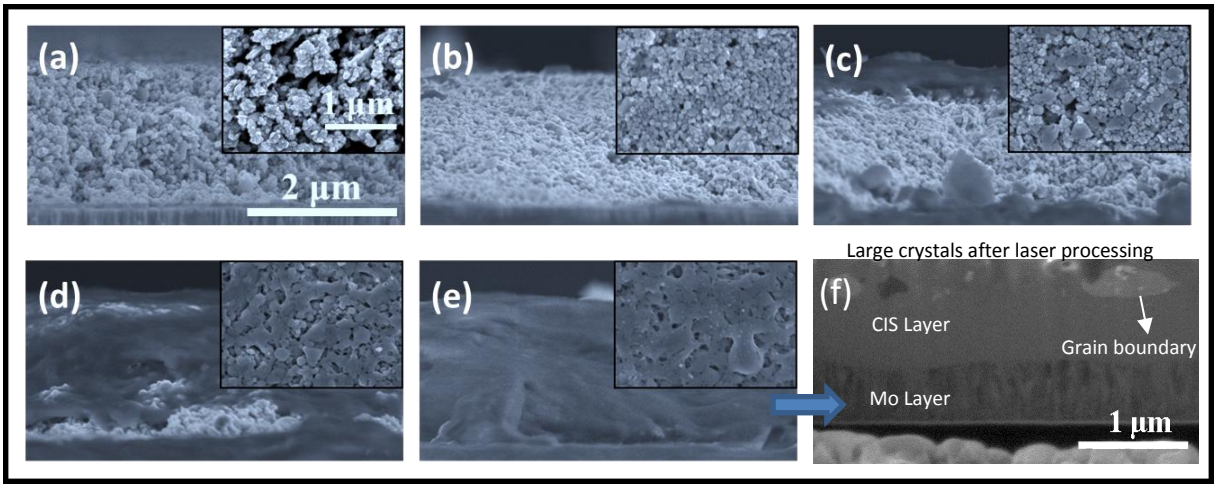

RSC Advances Accepted Manuscript

Figure 4

Multiphysics modeling showing the localized heating effects between the nanocrystals. (a) Laser beam local field concentration up to 14 V/m at nanoparticle contacts simulated by Comsol Multiphysics® with a Gaussian electromagnetic wave as incident beam on closely-packed CIS nanoparticles film. Gaussian beam laser was delivered with a setting field of 1 V/m. (b) 2 dimensional heat generation contours of close-packed CIS nanoparticles, calculated by power loss density in Comsol Multiphysics®. The unit is W/m^3.

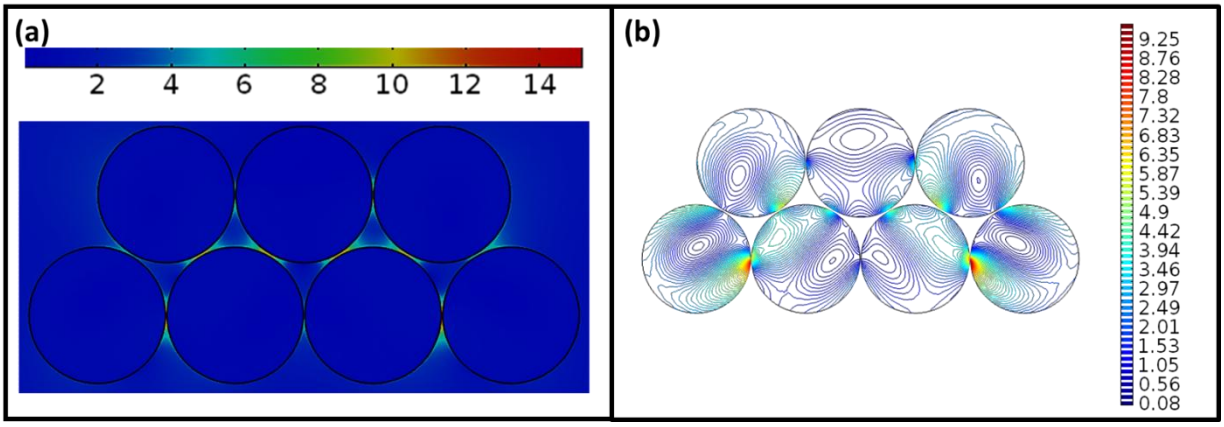

RSC Advances Accepted Manuscript

Figure 5

Figure 5: (a) Visible-near infrared absorbance (A) spectra of as-received and DPLC processed CIS absorber materials; insert illustrates the XRD spectrum of CIS after DPLC process. (b) expanded view of the NIR region showed an enhancement in absorbance; (c) The band gap (Eg) of the CIS thin film nanocrystals is approximated using the direct band gap method by plotting the absorbance squared versus energy, and extrapolating to zero as shown.

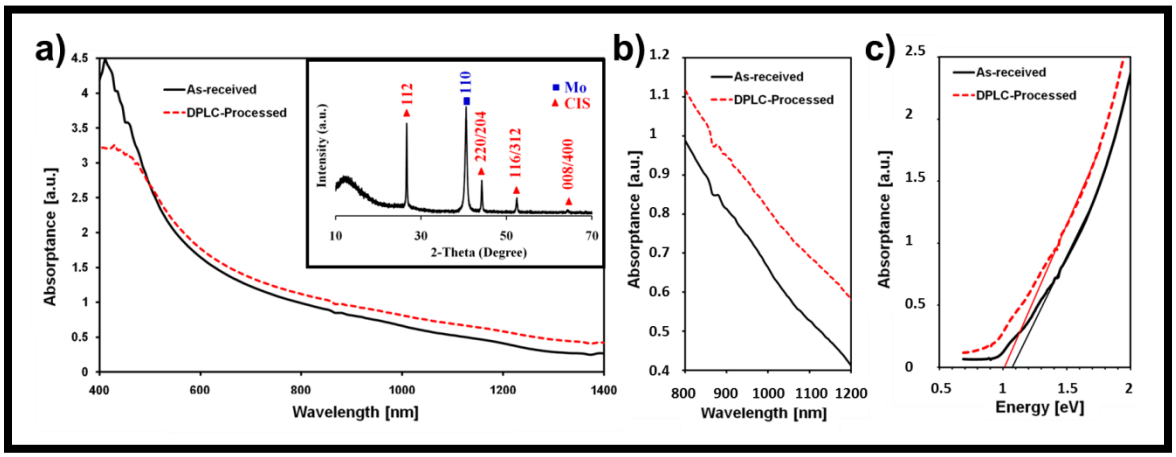

RSC Advances Accepted Manuscript

Figure 6

Figure7: (a) Raman spectra of CIS film recrystallized with different laser intensities; (b) Effect of pulse number of 3.8 MW/cm^2 (c) Effect of pulse number of 4.8 MW/cm^2 (d) Effect of pulse number of5.4 MW/cm^2 (e) Effect of pulse number affected by Laser intensity

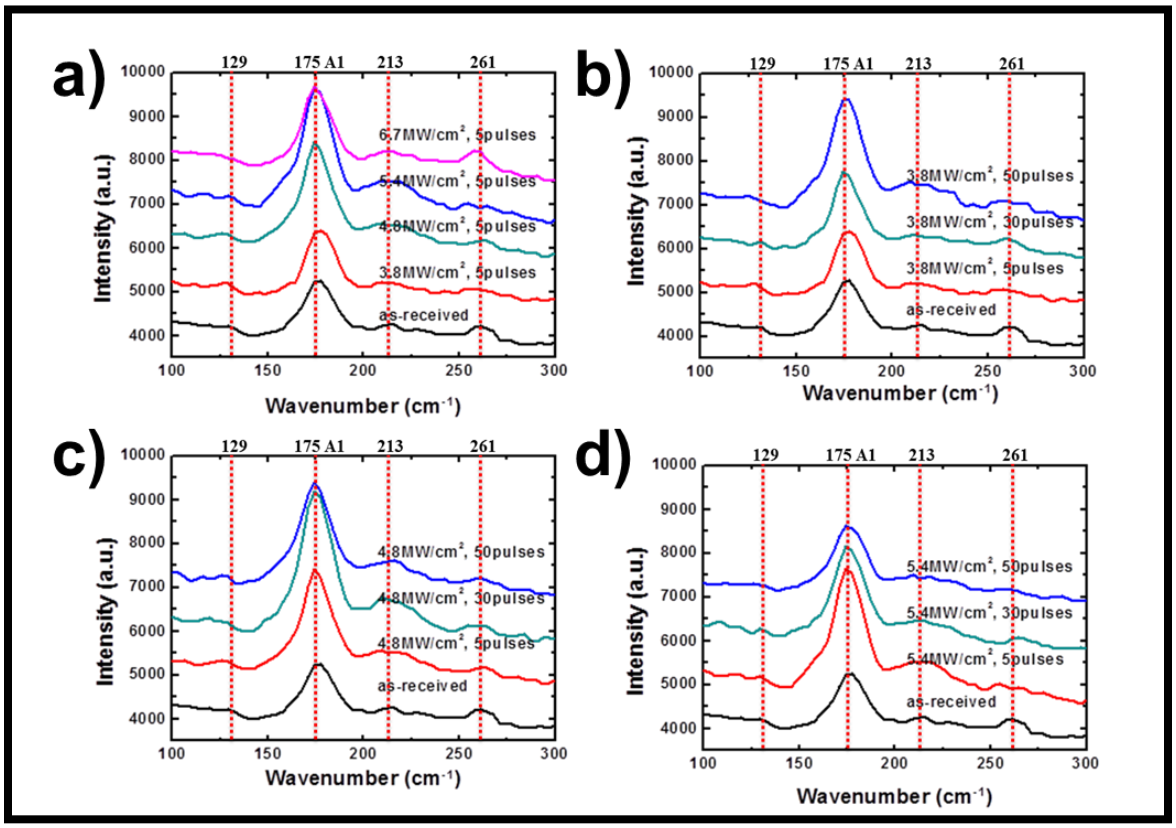

RSC Advances Accepted Manuscript

Figure 7

Figure 7: (a) PL spectra of CIS film recrystallized in different laser intensities; (b) Effect of pulse number of 3.8 MW/cm^2 (c) Effect of pulse number of 4.8 MW/cm^2 (d) Effect of pulse number affected by laser intensity

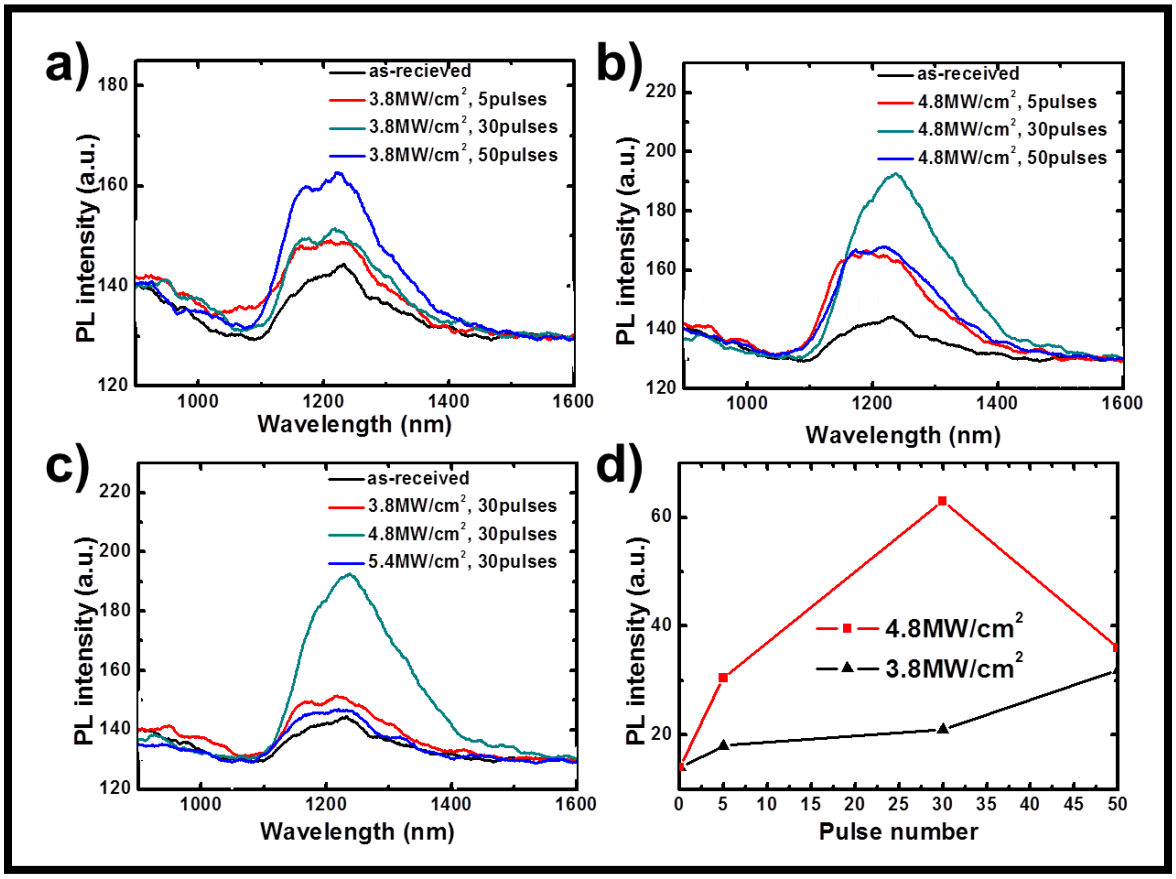

RSC Advances Accepted Manuscript

Reference

1. I. Repins, M. Contreras, M. Romero, Y. Yanfa, W. Metzger, J. Li, S. Johnston, B. Egaas, C. DeHart, J. Scharf, B. E. McCandless and R. Noufi, 2008.
2. B. J. Stanbery, *Crit. Rev. Solid State Mater. Sci.*, 2002, **27**, 73-117.
3. Q. Guo, S. J. Kim, M. Kar, W. N. Shafarman, R. W. Birkmire, E. A. Stach, R. Agrawal and H. W. Hillhouse, *Nano Lett.*, 2008, **8**, 2982-2987.
4. G. M. Ford, Q. Guo, R. Agrawal and H. W. Hillhouse, *Thin Solid Films*, 2011, **520**, 523-528.
5. M. E. Beck and M. Cocivera, *Thin Solid Films*, 1996, **272**, 71-82.
6. M. Graetzel, R. A. Janssen, D. B. Mitzi and E. H. Sargent, *Nature*, 2012, **488**, 304-312.
7. I. Sanyal, K. K. Chattopadhyay, S. Chaudhuri and A. K. Pal, *J. Appl. Phys.*, 1991, **70**, 841-845.
8. G. A. Kachurin, N. B. Pridaehin and L. S. Jmimov, *Fiz. Tekh. Poluprov*, 1975, **9**, 1429.
9. P. Baeri and E. Rimini, *Mater. Chem. Phys.*, 1996, **46**, 169-177.
10. J. Kim, Z. Hong, G. Li, T.-b. Song, J. Chey, Y. S. Lee, J. You, C.-C. Chen, D. K. Sadana and Y. Yang, *Nature communications*, 2015, **6**.
11. L. Dou, W. H. Chang, J. Gao, C. C. Chen, J. You and Y. Yang, *Adv. Mater.*, 2013, **25**, 825-831.
12. H. S. Duan, W. Yang, B. Bob, C. J. Hsu, B. Lei and Y. Yang, *Adv. Funct. Mater.*, 2013, **23**, 1466-1471.
13. J. Kim, H. Hiroi, T. K. Todorov, O. Gunawan, M. Kuwahara, T. Gokmen, D. Nair, M. Hopstaken, B. Shin and Y. S. Lee, *Adv. Mater.*, 2014, **26**, 7427-7431.
14. T. Todorov, H. Sugimoto, O. Gunawan, T. Gokmen and D. B. Mitzi, *Photovoltaics, IEEE Journal of*, 2014, **4**, 483-485.
15. M. Graetzel, R. A. Janssen, D. B. Mitzi and E. H. Sargent, *Nature*, 2012, **488**, 304-312.
16. Q. Nian, M. Y. Zhang, Y. Wang, S. R. Das, V. S. Bhat, F. Huang and G. J. Cheng, *Appl. Phys. Lett.*, 2014, **105**, -.
17. Q. Nian, M. Y. Zhang, B. D. Schwartz and G. J. Cheng, *Appl. Phys. Lett.*, 2014, **104**, -.
18. M. Y. Zhang and G. J. Cheng, *J. Appl. Phys.*, 2010, **108**, 113112-113119.
19. D. L. Barr and W. L. Brown, Scottsdale, Arizona (USA), 1995.
20. D. L. Barr, L. R. Harriott and W. L. Brown, Orlando, Florida (USA), 1992.
21. R. Fouret, B. Hennion, J. Gonzalez and S. Wasim, *Physical Review B*, 1993, **47**, 8269.
22. D. Haneman, *Critical Reviews in Solid State and Material Sciences*, 1988, **14**, 377-413.
23. H. Qian, Y. Ma, Q. Yang, B. Chen, Y. Liu, X. Guo, S. Lin, J. Ruan, X. Liu, L. Tong and Z. L. Wang, *ACS Nano*, 2014, DOI: 10.1021/nn406221s.
24. M. Song, G. Chen, Y. Liu, E. Wu, B. wu and H. Zeng, *Opt. Express*, 2012, **20**, 22290-22297.
25. G. Baffou, R. Quidant and C. Girard, *Appl. Phys. Lett.*, 2009, **94**, 153109.
26. M. Y. Zhang, Q. Nian, Y. Shin and G. J. Cheng, *J. Appl. Phys.*, 2013, **113**, 193506.
27. M. Y. Zhang, Q. Nian and G. J. Cheng, *Appl. Phys. Lett.*, 2012, **100**, 151902-151902-151904.
28. J. P. Kruth, X. Wang, T. Laoui and L. Froyen, *Assembly Automation*, 2003, **23**, 357-371.
29. P. Baeri, S. U. Campisano, G. Foti and E. Rimini, *J. Appl. Phys.*, 1979, **50**, 788-797.
30. C. V. Thompson and R. Carel, *J. Mech. Phys. Solids*, 1996, **44**, 657-673.
31. H. J. Frost, C. V. Thompson and D. T. Walton, *Acta Metallurgica et Materialia*, 1992, **40**, 779-793.
32. D. Pirzada and G. J. Cheng, *J. Appl. Phys.*, 2009, **105**, 093114-093117.
33. T. Savage and A. M. Rao, in *Thermal Conductivity*, ed. T. Tritt, Springer US, 2004, DOI: 10.1007/0-387-26017-X_12, ch. 12, pp. 261-284.
34. A. J. Kulkarni and M. Zhou, *Appl. Phys. Lett.*, 2006, **88**, 141921-141923.
35. A. J. Kulkarni, M. Zhou and F. J. Ke, *Nanotechnology*, 2005, **16**, 2749.
36. S. E. Aw, H. S. Tan and C. K. Ong, *J. Phys.: Condens. Matter*, 1991, **3**, 8213.

RSC Advances Accepted Manuscript

37. E. Burstein, *Phys. Rev.*, 1954, **93**, 632-633.
38. T. S. Moss, *Proceedings of the Physical Society. Section B*, 1954, **67**, 775.
39. H. Tanino, T. Maeda, H. Fujikake, H. Nakanishi, S. Endo and T. Irie, *Physical Review B*, 1992, **45**, 13323-13330.
40. C. Rincón and G. Sánchez Pérez, *Solid State Commun.*, 1984, **50**, 899-901.
41. E. P. Zaretskaya, V. F. Gremenok, V. Riede, W. Schmitz, K. Bente, V. B. Zalesski and O. V. Ermakov, *J. Phys. Chem. Solids*, 2003, **64**, 1989-1993.
42. C. Rincon and F. J. Ramirez, *J. Appl. Phys.*, 1992, **72**, 4321-4324.
43. J. H. Park, I. S. Yang and H. Y. Cho, *Appl. Phys. A*, 1994, **58**, 125-128.
44. S. Yamanaka, M. Konagai and K. Takahashi, *Jpn. J. Appl. Phys.*, 1989, **28**, L1337.
45. P. Lange, H. Neff, M. Fearheiley and K. J. Bachmann, *Physical Review B*, 1985, **31**, 4074-4076.
46. S. Shirakata and T. Nakada, *physica status solidi (c)*, 2009, **6**, 1059-1062.
47. J. F. Guillemoles, A. Lusson, P. Cowache, S. Massaccesi, J. Vedel and D. Lincot, *Adv. Mater.*, 1994, **6**, 376-379.
48. M. Y. Zhang and G. J. Cheng, *Appl. Phys. Lett.*, 2011, **99**, 051904-051903.

RSC Advances Accepted Manuscript

Direct pulsed laser crystallization (DPLC) is explored to rapidly crystallize large area coated copper indium diselenide (CIS) nanoparticle-inks.

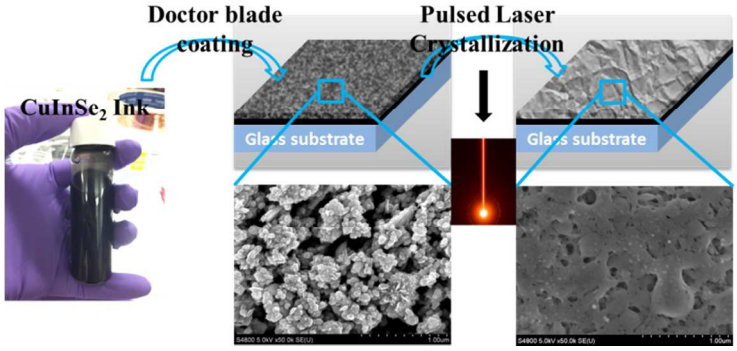

RSC Advances Accepted Manuscript